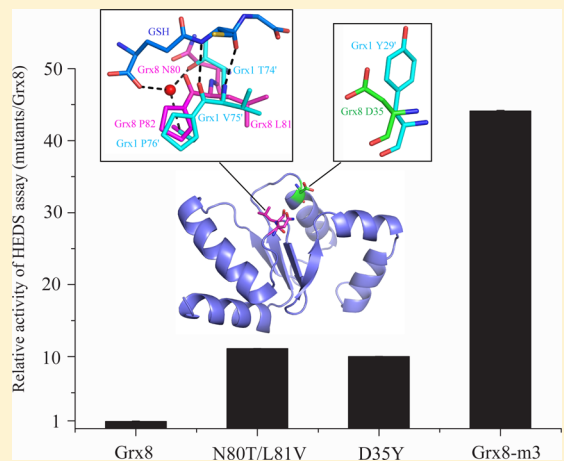


Structure-Guided Activity Enhancement and Catalytic Mechanism of Yeast Grx8

YaJun Tang, Jiahai Zhang, Jiang Yu, Ling Xu, Jihui Wu, Cong-Zhao Zhou,* and Yunyu Shi*

Hefei National Laboratory for Physical Sciences at the Microscale, School of Life Sciences, University of Science and Technology of China, Hefei, Anhui 230027, People's Republic of China

ABSTRACT: Glutaredoxins (Grxs) are wide-spread oxidoreductases that are found in all kingdoms of life. The yeast *Saccharomyces cerevisiae* encodes eight Grxs, among which, Grx8 shares a sequence identity of 30 and 23% with typical dithiol Grx1 and Grx2, respectively, but it exhibits a much lower GSH-dependent oxidoreductase activity. To elucidate its catalytic mechanism, we solved the solution structure of Grx8, which displays a typical Grx fold. Structural analysis indicated that Grx8 possesses a negatively charged CXXC motif ($\text{Cys}^{33}\text{-Pro}^{34}\text{-Asp}^{35}\text{-Cys}^{36}$) and a GSH-recognition site, which are distinct from Grx1 and Grx2. Subsequent structure-guided site mutations revealed that the D35Y single mutant and N80T/L81V double mutant possess increased activity of 10- and 11-fold, respectively; moreover, the D35Y/N80T/L81V triple mutant has increased activity of up to 44-fold, which is comparable to that of canonical Grx. Biochemical analyses suggested that the increase in catalytic efficiency resulted from a decreased pK_a value of catalytic cysteine Cys33 and/or enhancement of the putative GSH-recognition site. Moreover, NMR chemical shift perturbation analyses combined with GSH analogue inhibition assays enabled us to elucidate that wild-type Grx8 and all mutants adopt a ping–pong mechanism of catalysis. All together, these findings provide structural insights into the catalytic mechanism of dithiol Grxs.



Glutaredoxins (Grxs) have been characterized as a superfamily of the thioredoxin-fold oxidoreductases that possess a moderately conserved catalytic center, a CXXC/S motif. Grxs execute diverse biological functions, including defense against oxidative damage induced by different reactive oxygen species (ROS)¹ and sulfur (Fe–S) cluster assembly in response to cellular iron availability.² Grxs catalyze the reduction of mixed disulfides between proteins or low-molecular-weight thiols and reduced glutathione (GSH) in the presence of NADPH, GSH, and glutathione reductase.³ It has been demonstrated that because of its low pK_a value, the N-terminal cysteine of Grxs becomes a good nucleophile and leaving group during the catalytic reaction.^{4–7} Grxs can be grouped into monothiol and dithiol Grxs according to the number of active-site cysteine residues in the CXXC/S motif. The conserved active-site motifs are usually CPYC in the classical dithiol Grxs and CGFS in the monothiol Grxs. Most members of the Grx family are capable of binding to GSH via a mixed disulfide bond in addition to extensive hydrogen bonds and electrostatic and hydrophobic interactions.^{8–10}

Kinetic analyses suggested that Grxs might have two different catalytic mechanisms: ping–pong and sequential.^{6,11–15} In the proposed ping–pong mechanism, the first substrate binds to Grxs followed by formation of an intermediate and subsequent release of the first product; the second substrate then reacts with Grxs, resulting in the formation of the final product. In

contrast, the sequential mechanism hypothesizes that the two substrates simultaneously bind to Grxs. In the case of human Grx2, kinetics analysis revealed a ping–pong mechanism when using BSA–SSG and GSH as the two substrates.⁶ Similarly, GrxS12 also adopts a ping–pong mechanism toward BSA–SSG and GSH.¹¹ However, the classic dithiol Grxs, yeast Grx1 and Grx2, demonstrate a sequential mechanism toward β -hydroxyethyl disulfide (HEDS) and GSH.¹⁵ Moreover, human Grx utilizes a ping–pong mechanism toward GS-SCys (L-cysteine-glutathione disulfide) and GSH¹² and a sequential mechanism toward HEDS and GSH.¹³ A similar switch in the catalytic mechanism has been found for yeast Grx7.¹⁴ In contrast to the clearly described ping–pong mechanism, the sequential mechanism toward HEDS that has been proposed in a few papers remains uncertain.¹⁴

The baker's yeast *Saccharomyces cerevisiae* encodes eight Grxs, including three dithiol Grxs and five monothiol Grxs. Dithiol Grx1/YCL035C and Grx2/YDR513W share a high degree of sequence identity (64%) but quite different GSH-dependent oxidoreductase activity because of their different active-site structures.¹⁵ In addition, we have demonstrated that variations of the residues at the GSH-recognition site also contribute to

Received: September 21, 2013

Revised: February 19, 2014

Published: March 10, 2014



the difference in their enzymatic activity.¹⁶ The five monothiol Grxs include Grx3/YDR098C, Grx4/YER174C, Grx5/YPL059W, Grx6/YDL010W, and Grx7/YBR014C.^{17–19} Notably, both Grx6 and Grx7 show a much higher HEDS activity compared to that of previously reported monothiol Grxs.¹⁴ We have solved the crystal structures of yeast Grx1, Grx5, and Grx6 and compared their enzymatic activities.^{9,20} These analyses revealed the diversity of Grxs from both structural and catalytic points of view, even for yeast Grx1 to Grx8, which are encoded by a same organism.^{14–16,20}

As the third dithiol Grx recently reported in *S. cerevisiae*,¹⁸ Grx8 was found to be unnecessary in the defense against general oxidative stress despite its localization in the cytosol.²¹ Grx8 displays a very low Grx activity *in vitro*; moreover, a flanking tryptophane residue at the CPDC motif (Trp³²-Cys³³-Pro³⁴-Asp³⁵-Cys³⁶) makes it more likely to be a thioredoxin. Here, we have solved the solution structure of Grx8 and found that it indeed adopts an overall structure of a Grx. Multiple-sequence alignment combined with NMR titration assays enabled us to assign the key residues contributing to the differences between Grx8 and the other two yeast dithiol Grxs. Subsequent site-directed mutageneses combined with activity assays revealed that Asp35 in the CPDC motif and residues Asn80 and Leu81 are involved in the high pK_a value of the active-site cysteine and GSH-recognition site, respectively. On the basis of NMR chemical shift perturbation and GSH analogue inhibition assays, we found that wild-type Grx8 and its mutants adopt a ping-pong mechanism of catalysis toward HEDS and GSH. Moreover, we propose that the previous sequential mechanism observed in a two-substrate kinetics model might be due to the rate-limiting formation of the real substrate, β-ME-SSG, and/or the accelerated formation of glutathionylated Grxs. Our findings provide novel insights into the relationship between the structural motifs and catalytic mechanisms of Grxs.

EXPERIMENTAL PROCEDURES

Plasmids Construction. The coding region of the yeast Grx8 gene was PCR-amplified using yeast genomic DNA as the template and cloned into the p28 expression vector. The p28 vector is modified from the pET28a(+) (Novagen) plasmid, and NdeI and XhoI were used as cloning sites, giving an N-terminal MGHHHHHH tag. All Grx8 mutants were generated using the QuikChange mutagenesis kit (Takara) and confirmed by DNA sequencing. Grx8-m3 stands for the D35Y/N80T/L81V triple mutant.

Expression, Purification, and Isotope Labeling of the Recombinant Protein. All plasmids with the coding sequence for an N-terminal 6× His tag were transformed into *Escherichia coli* Rosetta (DE3) competent cells. Bacteria harboring the recombinant Grx8 or its mutants were cultivated in 2× YT medium containing 50 μg/mL of kanamycin and 34 μg/mL of chloromycetin and were induced with 0.2 mM isopropyl β-D-1-thiogalactopyranoside (IPTG) at 37 °C for 4 h after the OD_{600nm} reached 0.8. Uniformly ¹⁵N- or ¹⁵N/¹³C-labeled recombinant Grx8 was produced by using ¹⁵NH₄Cl (0.5 g/L) and/or ¹³C-D-glucose (2.5 g/L) as the sole nitrogen and carbon sources. Labeled proteins were expressed in M9 medium and induced with 0.2 mM IPTG at 37 °C for 6 h. The harvested cells were resuspended in 40 mL of buffer containing 20 mM Tris-HCl, pH 7.5, 200 mM NaCl, and 14 mM β-mercaptoethanol and sonicated for 12 min. The supernatant was then applied to a Ni-chelating column (Qiagen) following

the manufacturer's protocol. The recombinant proteins were eluted with buffer containing 500 mM imidazole. The eluate was concentrated to 5 mL by a Millipore Amicon Ultra 15 mL centrifugal filter device. Samples were further purified by gel-filtration chromatography on a Superdex 75 column (GE Healthcare) that was pre-equilibrated with buffer (20 mM Tris-HCl, pH 8.0, 200 mM NaCl, and 14 mM β-mercaptoethanol). Protein concentration was assessed by ultraviolet (UV) absorbance spectra at 280 nm with the following extinction coefficients: ε_{Grx8} = 24 980, ε_{N80T/L81V} = 24 980, ε_{D35Y} = 26 470, ε_{Grx8-m3} = 26 470, ε_{E94N/S95D/Q96D} = 24 980, ε_{R69Q} = 24 980, and ε_{C36S} = 24 980.

NMR Spectroscopy and Data Processing. The purified ¹⁵N- and ¹⁵N/¹³C-labeled proteins were dissolved to a final concentration of 0.8 mM in 500 μL of buffer containing 20 mM phosphate sodium, pH 5.6, 50 mM NaCl, 2 mM EDTA, and 5 mM DTT in a 90% H₂O and 10% D₂O mixture or in 99.96% D₂O. All of the NMR experiments were performed at 303 K on a Bruker DMX500 or DMX600 spectrometer. The following spectra were recorded with self-shielded Z-axis gradients to obtain the backbone and side-chain resonance assignments: 2D ¹H-¹⁵N HSQC and 3D HNCO, HN(CA)CO, CBCA(CO)-NH, CBCANH, (H)C(CO)NH-TOCSY, HBHA(CBCA)-(CO)NH, H(C)(CO)NH-TOCSY, HCCH-COSY, and HCCH-TOCSY. After HSQC spectra, the ¹⁵N-labeled protein was lyophilized and dissolved in 99.96% D₂O. HSQC spectra were immediately collected to record the disappearance of NH signals and to identify the slowly exchanging amides. NMR data were processed using NMRPipe and NMRDraw software²² and analyzed with Sparky3 software.²³ The resonances of the ¹⁵N-¹H HSQC spectra of the C36S and N80T/L81V mutants were assigned using 3D ¹H, ¹⁵N-edited NOESY-HSQC spectra.

For titration experiments, GSH and GSSG (BBI Bio, Inc.) were dissolved in buffer containing 20 mM phosphate sodium, pH 5.6, 50 mM NaCl, and 2 mM EDTA to prepare a 200 mM solution. NMR titration experiments were performed by adding increasing amounts of unlabeled GSH to ¹⁵N-labeled Grx8 or the N80T/L81V mutant, respectively. A series of 2D ¹H-¹⁵N HSQC spectra were recorded at protein/GSH mole ratios of 1:111, 1:222, 1:311, and 1:378. GSSG was titrated to the ¹⁵N-labeled C36S mutant, and the C36S mutant/GSSG mole ratios were 1:0.2, 1:0.5, 1:1, 1:2, and 1:5.

Measurement of Equilibrium Dissociation Constants. Dissociation constants of Grx8 or the N80T/L81V mutant were obtained by monitoring the chemical shift changes from the unbound to bound forms during GSH titration. Combined chemical shift perturbation was calculated using the following equation

$$\Delta\delta = \sqrt[3]{(\Delta\delta_{HN})^2 + (0.17\Delta\delta_N)^2}$$

where Δδ_{HN} and Δδ_N are the chemical shift variations in the proton and nitrogen dimensions, respectively. The dissociation constant, K_d, value was fitted using the following equation

$$\Delta\delta = \frac{\Delta\delta_{\max}}{2[P_0]} \left(K_d + (n + 1)[P_0] - \sqrt[3]{((n + 1)[P_0] + K_d)^2 - 4n[P_0]^2} \right)$$

where $\Delta\delta_{\max}$ is the chemical shift of the protein fully saturated with GSH, P_0 is the concentration of protein, and n is the molar ratio of GSH to protein.

NMR Structure Calculation and Validation. NOE distance restraints were obtained from 3D ^{15}N - and ^{13}C -separated NOESY spectra. Backbone dihedral angle restraints (φ and ψ) of secondary structures were derived from the analysis of $^{13}\text{C}\alpha$, $^{13}\text{C}\beta$, ^{13}CO , $^1\text{H}\alpha$, and ^{15}N chemical shifts by the TALOS+ program.²⁴ Hydrogen-bond restraints were added on the basis of the slow-exchanging amide protons of the α -helix and β -sheet. The structures were calculated using the CNS1.2 program²⁵ with 1813 NOE distance restraints, 97 backbone dihedral angle restraints, and 36 hydrogen-bond restraints. In the initial stage of calculation, only unambiguous NOE distance restraints of the sequential, medium-range, and dihedral angle restraints were introduced. Then, the long-range NOEs and hydrogen bonds were added into the calculation files. In the final calculation stage, 200 structures were generated, and 20 conformers with the lowest energies were selected to form the representative ensemble. Structural quality was validated by the PROCHECK program.²⁶ Molecular graphics were visualized by MOLMOL²⁷ and PyMOL (<http://www.pymol.org>).

HEDS Assays. Glutathionyl mixed disulfide reductase activity of Grx8 and the D35Y, N80T/L81V, Grx8-m3, R69Q, and E94N/S95D/Q96D mutants were measured with the standard HEDS assays for Grxs, at 20 °C, using a mixed disulfide between HEDS and GSH as the substrate with a DU800 UV-vis spectrophotometer (Beckman Coulter, Fullerton, CA, USA).³ Solutions of 25 mM NADPH, 200 mM GSH, 0.6 mg/mL of yeast glutathione reductase (GR) (Sigma-Aldrich), and 70 mM HEDS (Sigma-Aldrich) were freshly prepared. The reaction mixture contained 100 mM Tris-HCl, pH 7.5, 0.125 mM NADPH, 2.0 mM GSH, 6.0 µg/mL of GR, 1 mM HEDS, and various concentrations of Grx8 or its mutants. The final concentrations of Grx8 and its mutants (D35Y, N80T/L81V, and Grx8-m3) were 22.5, 2.25, 2.5, and 1.0 µM, respectively. GSH and HEDS were preincubated for 3 min to form the mixed disulfide. The reaction was triggered by the addition of the wild-type Grx8 or mutants. The decrease in the absorbance at 340 nm because of the oxidation of NADPH was recorded. In all HEDS assays, the velocities of the control reactions without enzymes were subtracted to correct the measured activities. Three independent experiments were performed for each substrate concentration.

To determine the kinetic parameters of Grx8 and its mutants toward HEDS, 0.1–2.0 mM HEDS was added in a mixture of 100 mM Tris-HCl, pH 7.5, 0.125 mM NADPH, 2.0 mM GSH, and 6.0 µg/mL of GR. The reaction was triggered by adding different concentrations of Grx8 or mutants. The final concentrations of the enzymes in the reaction mixture were 22.5 µM Grx8, 2.25 µM D35Y mutant, 2.5 µM N80T/L81V mutant, or 1.0 µM Grx8-m3. To determine the kinetic parameters of Grx8 and its mutants for GSH, 0.5–3.5 mM GSH was added to the reaction mixture containing 100 mM Tris-HCl, pH 7.5, 0.125 mM NADPH, 0.7 mM HEDS, and 6.0 µg/mL of GR. The final concentrations of the enzymes were 22.5 (Grx8), 2.0 (D35Y mutant), 2.5 (N80T/L81V mutant), and 0.9 µM (Grx8-m3). Independent experiments were performed three times at each substrate concentration. The apparent K_m^{app} and $k_{\text{cat}}^{\text{app}}$ values were calculated by nonlinear regression of Michaelis-Menten plots.

Determination of the $\text{p}K_a$ Value of the N-Terminal Cysteine. The $\text{p}K_a$ value of the N-terminal cysteine was determined by a monobromobimane alkylation method that generates a fluorescent product ($\lambda_{\text{exc}} = 396$ nm and $\lambda_{\text{em}} = 482$ nm) independently.¹⁵ Purified Grx1, Grx8, and the D35Y mutant were previously reduced by 0.1 mM DTT for 2 h in the presence of 0.1 mM diethylenetriamine pentaacetic acid at room temperature. Excess DTT was then removed by size-exclusion chromatography (HiLoad 16/60 Superdex 75 column, GE Healthcare) equilibrated with buffer (20 mM Tris-HCl, pH 8.0, and 200 mM NaCl). Protein concentrations were determined using the extinction coefficient ($\epsilon_{\text{Grx1}} = 5960$, $\epsilon_{\text{Grx8}} = 24\,980$, and $\epsilon_{\text{D35Y}} = 26\,470$) at 280 nm. Grx1 (10 µM), Grx8 (120 µM), and the D35Y mutant (120 µM) were incubated with monobromobimane (6.0 µM) in buffer at various pH values in 96-well plates. The concentration of the buffers (KCl-HCl, pH 1.53; citrate-phosphate, pH 2.49, 3.06, 3.48, 4.03, 4.46, and 4.97; MES-NaOH, pH 5.52, 6.01, and 6.51; and Tris-HCl, pH 6.92, 7.52, 8.05, 8.49, and 9.05) was 50 mM. The ionic strength of the buffers was adjusted to 0.5 M by the addition of NaCl. The absorbance was recorded by a SpectraMax M5 plate reader (Molecular Devices). The mixture containing all of the components except for the protein was used as the control. The rates of monobromobimane alkylation were plotted versus pH values, and the $\text{p}K_a$ value was fitted by sigmoidal dose-response curves

$$\text{rate of alkylation} = \text{rate}_{\text{bottom}} + \frac{\text{rate}_{\text{top}} - \text{rate}_{\text{bottom}}}{1 + 10^{\frac{((\text{p}K_a - \text{pH}) \cdot \text{Hill slope})}{2}}}$$

The Hill slope is equal to 1.00. $\text{rate}_{\text{bottom}}$ and rate_{top} represent the lowest and highest rate in the monobromobimane alkylation reaction, respectively. The values of $\text{p}K_a$, $\text{rate}_{\text{bottom}}$, and rate_{top} are fitted with Origin8.5 software.

GST Assays. According to the method using NBD-Cl and GSH as substrates,²⁸ GST activity was assayed by detection of the produced yellow compound at 419 nm with a DU800 spectrophotometer. 50 mM NBD-Cl and 200 mM GSH were freshly prepared as stock solutions. The reaction mixture contained 0.1 M sodium acetate buffer, pH 5.0, 0.5 mM NBD-Cl, 1 mM GSH, and 10 µM protein. Independent experiments were performed three times.

Two-Substrate Kinetics. By varying the concentration of HEDS from 0.1 to 2.0 mM at fixed concentrations of GSH (1.0, 1.5, or 2.0 mM), two-substrate kinetics were performed at 20 °C. The components of the reaction mixture were the same as that of the HEDS assays. The final concentrations of the enzyme in the reaction mixture were 22.5 µM Grx8, 2.25 µM D35Y mutant, 2.5 µM N80T/L81V mutant, or 1.0 µM Grx8-m3. K_m^{app} and V_m^{app} values were calculated in the same manner as described for the HEDS assay. The reciprocal of the V_m^{app} values was plotted versus the reciprocal of GSH concentrations to provide the true K_m value for GSH.

RESULTS

Grx8 Possesses a Very Low HEDS Activity. Dithiol Grxs are capable of catalyzing the GSH-dependent reduction of β -hydroxyethyl disulfide (HEDS) to β -mercaptoethanol in a coupled enzymatic assay. Consistent with a previous report,²¹ we found that Grx8 exhibits a detectable enzymatic activity toward HEDS only at micromolar concentration. Furthermore, we determined the kinetic parameters of Grx8. At a fixed concentration of GSH, the apparent kinetic data could be well-

Table 1. Apparent Steady-State Kinetic Data of Grx8 and Its Mutants for HEDS and GSH

protein	HEDS			GSH		
	K_m^{app} (mM) ^a	K_{cat}^{app} ($\times 10^{-3}$ s ⁻¹) ^a	K_{cat}^{app}/K_m^{app} (M ⁻¹ s ⁻¹) ^a	K_m^{app} (mM) ^b	K_{cat}^{app} ($\times 10^{-3}$ s ⁻¹) ^b	K_{cat}^{app}/K_m^{app} (M ⁻¹ s ⁻¹) ^b
Grx8	0.62 ± 0.11	11.50 ± 1.42	18.55 ± 5.58	2.02 ± 0.22	12.04 ± 0.66	5.99 ± 0.98
D35Y	1.62 ± 0.33	199 ± 16.3	122.83 ± 35.1	1.62 ± 0.14	129 ± 6.64	79.63 ± 11.0
N80T/L81V	2.89 ± 0.30	333 ± 32.0	115.22 ± 23.0	0.93 ± 0.15	57.60 ± 3.16	61.72 ± 13.3
Grx8-m3	2.30 ± 0.15	752 ± 44.7	326.96 ± 40.8	2.58 ± 0.13	467 ± 15.6	181.01 ± 15.2

^aThe reaction mixture contained 100 mM Tris-HCl (pH 7.5), 2 mM GSH, 0.125 mM NADPH, and 6 µg/mL of GR. The concentration of HEDS was varied from 0.1 to 2.0 mM at a fixed concentration of GSH, and the reactions were started by the addition of Grx8 or the mutants. ^bThe reaction mixture contained 100 mM Tris-HCl (pH 7.5), 0.7 mM HEDS, 0.125 mM NADPH, and 6 µg/mL of GR. The concentration of GSH was varied from 0.5 to 3.5 mM at a fixed concentration of HEDS, and the reactions were started by the addition of Grx8 or the mutants.

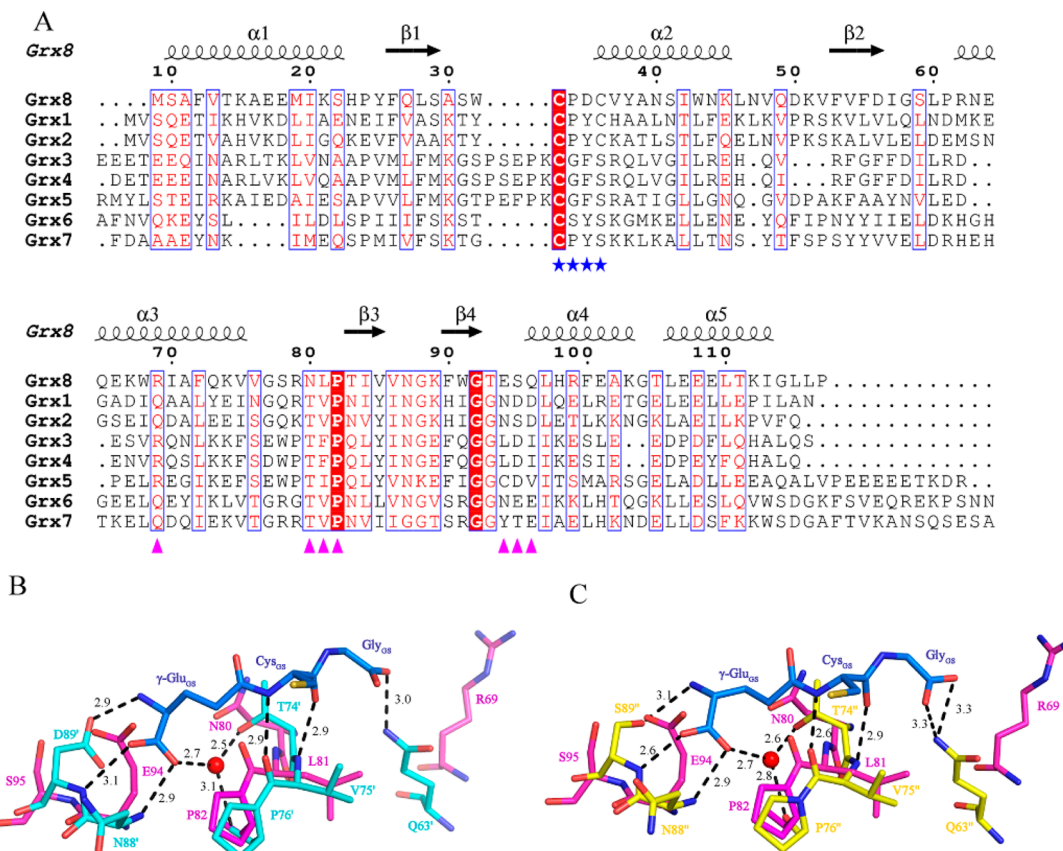


Figure 1. Comparison of Grx8 and the other two yeast dithiol Grxs. (A) Multiple-sequence alignment of the yeast Grxs. Grx1 (NP_009895), Grx2 (NP_010801), Grx3 (NP_010383), Grx4 (NP_011101), Grx5 (NP_015266), Grx6 (NP_010274), Grx7 (NP_009570), and Grx8 (NP_013468) sequences from *S. cerevisiae* were aligned using the Multalin program. Blue stars indicate residues of the CXXC motif. Residues at the GSH-recognition site are marked in magenta triangles. (B) Structural superposition of the GSH-recognition site of Grx8 with that of Grx1_{SG} (PDB 3C1S). The solution structure of Grx8 is magenta. The crystal structure of Grx1_{SG} complex is cyan. The glutathione moiety is blue. The red ball represents a water molecule. (C) Structural superposition of the GSH-recognition site of Grx8 with that of Grx2_{SG} (PDB 3D5J). The crystal structure of the Grx2_{SG} complex is yellow.

fitted to the Michaelis–Menten formula (Table 1). Grx8 has a K_m^{app} value toward HEDS of 0.62 mM and a k_{cat}^{app} value of 1.15×10^{-2} s⁻¹, resulting in a very low catalytic efficiency (k_{cat}^{app}/K_m^{app} in M⁻¹ s⁻¹), which is 3 orders of magnitude lower than those of yeast Grx1 or Grx2.¹⁵

The sequence alignment indicated that Grx8 shares 30 and 23% sequence identity with yeast Grx1 and Grx2, respectively (Figure 1A). The key alterations in Grx8 are at the active-site CXXC motif and GSH-recognition site. Grx8 employs a CPDC motif rather than the CPY(F)C motif found in the typical Grxs. In addition, the TVP motif in most Grxs that is involved in the

interactions with the cysteinyl moiety of GSH is substituted by residues Asn80, Leu81, and Pro82 in Grx8, whereas the Gln residue involved in stabilizing the glycine moiety of GSH is replaced by Arg69 in Grx8. Moreover, residues Glu94 and Ser95 of Grx8 correspond to Asn and Asp/Ser of Grx1/Grx2 that form intensive hydrogen bonds with the γ -glutamyl moiety of GSH.⁹ To determine whether these alterations influence the enzymatic activity and the molecular mechanism of catalysis by Grx8, we determined the solution structure of Grx8 by NMR.

Solution Structure of Grx8. The solution structure of Grx8 was determined by multidimensional heteronuclear NMR

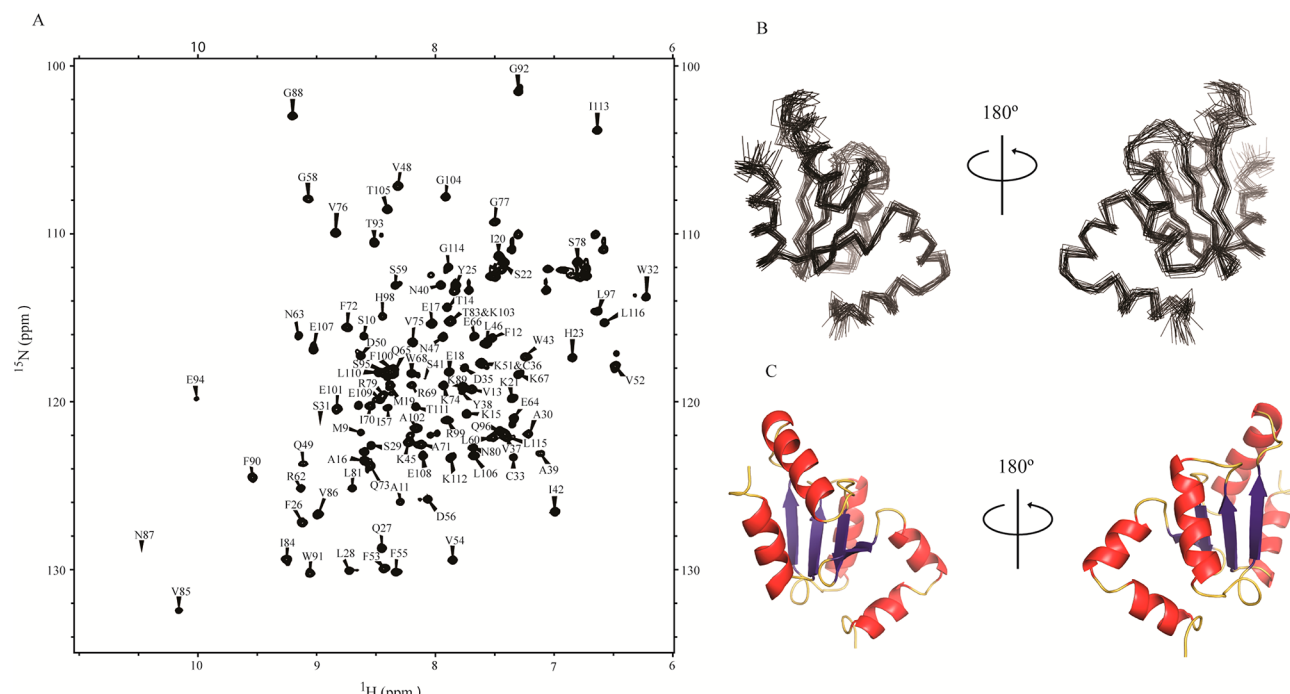


Figure 2. Solution structure of Grx8. (A) Two-dimensional ¹⁵N-¹H HSQC spectrum of Grx8. (B) Stereo view of the 20 structures of lowest energy superimposed for best fit of the N, CO, and CA atoms of residues 12–29, 35–56, and 65–112. (C) Cartoon representation of the solution structure of Grx8.

spectroscopy. The ¹⁵N-¹H HSQC experiment shows a dispersed spectrum of amide groups (Figure 2A), indicating a well-folded structure. The structure of Grx8 was calculated using CNS1.2 with 1813 NOE distance restraints, 97 backbone dihedral angle restraints, and 36 hydrogen-bond restraints. An ensemble of 20 structures of the lowest energy out of 200 calculated structures was determined and highly converged (Figure 2B). These 20 structures have a root-mean-square deviation (rmsd) of 0.768 Å for the backbone atoms. The structural data and statistics are listed in Table 2.

Grx8 contains a core β -sheet of four antiparallel β -strands, β_1 (Phe26–Ser29), β_2 (Phe53–Asp56), β_3 (Thr83–Val85), and β_4 (Phe90–Gly92), which is flanked by five α -helices, α_1 (Ser10–Ser22), α_2 (Cys36–Lys45), α_3 (Arg62–Val75), α_4 (Gln96–Lys103), and α_5 (Leu106–Ile113) (Figure 2C). A Dali search (http://ekhidna.biocenter.helsinki.fi/dali_server/) gave an output of 709 hits with a Z score > 3.0, most of which are thiol oxidoreductases. Yeast Grx6, Grx2, and Grx1 are listed as the top three hits, all of which have a Z score of about 11. This indicated that Grx8 also displays a canonical Grx fold similar to that of yeast Grx1 and Grx2.

The CPDC motif of Grx8 localizes at the N-terminus of helix α_2 and the preceding loop. The putative GSH-recognition motif (Arg69, Asn80–Leu81–Pro82, and Glu94–Ser95–Gln96) localizes at the middle of helix α_3 , the loop that precedes β_3 , and the loop that precedes helix α_4 , respectively.

Structural Comparison between Grx8 and the Other Two Yeast Dithiol Grxs. The dithiol Grx undergoes different redox states during the catalytic process. At the beginning, the reduced Grx (Grx_{re}) performs a nucleophilic attack at the glutathionylated substrate to form an intermediate glutathionylated Grx (Grx_{GS}). Upon the formation of an intramolecular disulfide bond between the two active-site cysteines, the Grx is switched to an oxidized form (Grx_{ox}).

Table 2. Structural Statistics for the 20 Energy-Refined Conformers of Grx8^a

Grx8	
NMR Restraints	
NOE distance restraints	1813
intraresidue	400
sequential ($ i - j = 1$)	600
medium range ($ i - j < 5$)	472
long range ($ i - j \geq 5$)	305
hydrogen bonds	36
dihedral angle restraints	97
Mean rmsd from Idealized Covalent Geometry	
bonds (Å)	0.003 ± 0.0002
angles (degrees)	0.332 ± 0.0058
improper (degrees)	0.155 ± 0.0082
Mean rmsd from Experiment Restraints	
distance (Å)	0.007 ± 0.001
Cdh (degrees)	0.174 ± 0.022
Structural rmsd to the Mean Coordinates (Å) ^b	
backbones atoms	0.768
heavy atoms	1.368
Ramachandran Plot Analysis (%) ^c	
residues in most favored regions	84.9
residues in additional allowed regions	14.3
residues in generously allowed regions	0.5
residues in disallowed regions	0.3

^aNone of the structures exhibited distance violations of >0.5 Å or dihedral angle violations of >5 rmsd, root-mean-square violation.

^brmsd was calculated using residues 12–29, 35–56, and 65–112, excluding the loop and disordered regions. ^cRamachandran plot of ordered residues was analyzed by PROCHECK.

The structures of yeast Grx1 and Grx2 in different oxidative states have been determined: Grx1_{re} (PDB code 2JAD),²⁹

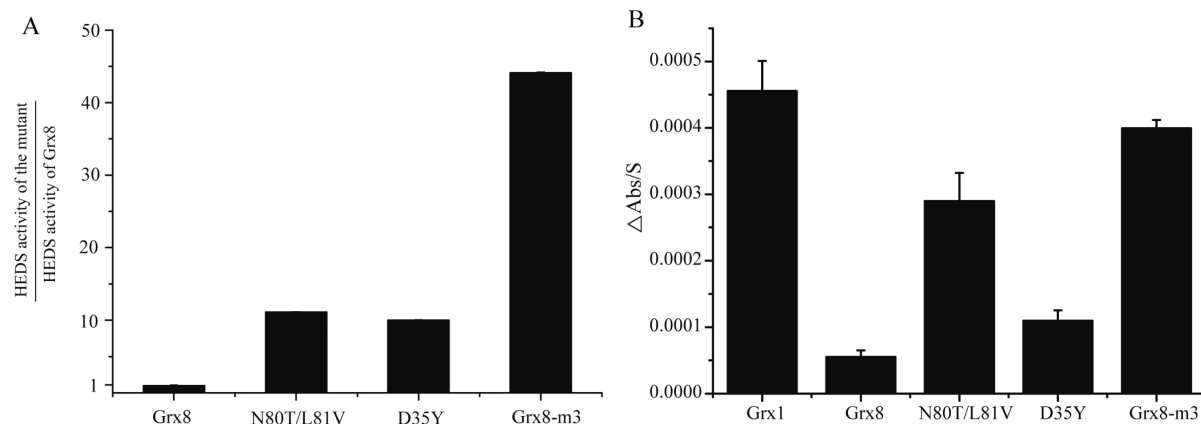


Figure 3. Enzymatic assays of Grx8 and its mutants. (A) HEDS assays. The reaction velocities of Grx8 and its mutants were calculated by $\text{OD}_{340}/T/[E]$. Histograms of enzymatic activity are shown by the ratio of the HEDS activity of the mutants and that of Grx8. (B) GST activities of Grxs and mutants.

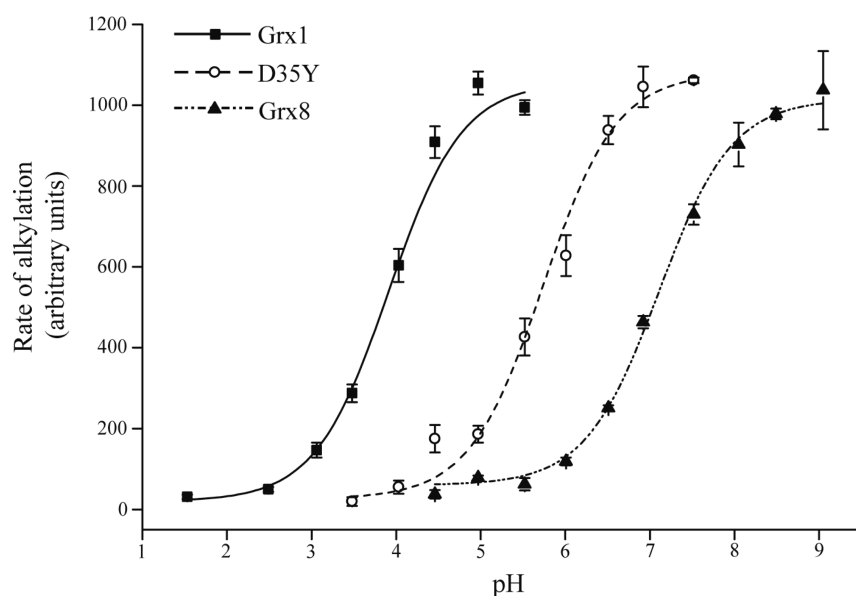


Figure 4. Determination of the $\text{p}K_a$ values of the N-terminal cysteine of Grx8, D35Y, and Grx1. Ten micromolar Grx1 (filled squares), 120 μM D35Y (open circles), or 120 μM Grx8 (filled triangles) was alkylated with 6 μM monobromobimane at different pH values at 20 °C, as described in the Experimental Procedures.

Grx2_{re} (PDB code 3CTG),¹⁶ Grx1_{GS} (PDB code 3C1S),⁹ Grx2_{GS} (PDB code 3D5J),¹⁵ Grx1_{ox} (PDB code 3C1R),⁹ and Grx2_{ox} (PDB code 3D4M).¹⁵ Structural comparison of Grx8 with these Grxs yielded an overall rmsd of 2.6–2.7 Å over about 104 $\text{C}\alpha$ atoms, respectively.

To focus on the difference at the GSH-recognition site first, we took glutathionylated yeast Grx1 and Grx2 as examples for superposition (Figure 1B,C). For the GSH-recognition sites of Grx1_{GS} and Grx2_{GS}, the amide nitrogen and carbonyl oxygen of the cysteinyl group of GSH form hydrogen bonds with the carbonyl oxygen and amide nitrogen of Val75, respectively (Figure 1B,C).^{9,15} The hydroxyl of Thr74' and carbonyl oxygen of Pro76' in Grx1 forms water-mediated hydrogen bonds with one of the oxygen atoms of the glutamyl moiety in GSH.⁹ The counterpart residues in Grx8 are Asn80 and Leu81, which have a slightly larger side chain compared to residues Thr74 and Val75 in Grx1 and Grx2. The steric hindrance may impede the formation of hydrogen bonds between GSH and Grx8 (Figure 1B,C). Concerning the residues of Grx1_{GS} and Grx2_{GS} that interact with the γ -Glu and Gly moieties of GSH, Asn88' and

Asp89'/Ser89'' correspond to Glu94 and Ser95 of Grx8, whereas Gln63' is substituted by Arg69 in Grx8 (Figure 1B,C).

In addition to the variations at the GSH-recognition site, another major difference is in the CXXC motif. Grx8 also has a CPDC motif located at the N-terminus of helix $\alpha 2$ and its preceding loop (Figure 1A), similar to that of most Grxs.^{15,30,31} However, the CPDC motif of Grx8 is significantly different from the CPYC motif in Grx1 and Grx2.

Mutation of D35Y Significantly Increases the GSH-Dependent Oxidoreductase Activity. To check whether Asp35 in the CPDC motif is responsible for the dramatically decreased GSH-dependent oxidoreductase activity of Grx8, we constructed a D35Y single mutant and compared its activity with the wild type. The apparent kinetic data toward HEDS or GSH was fitted by nonlinear regression of Michaelis–Menten plots (Table 1). As shown in Figure 3A, the D35Y mutation led to an increase of the GSH-dependent oxidoreductase activity of about 10-fold compared to that of the wild type. For HEDS, the $k_{\text{cat}}^{\text{app}}$ value of the D35Y mutant is 17.30-fold higher than that of the wild type, and its catalytic efficiency is increased 6.62-

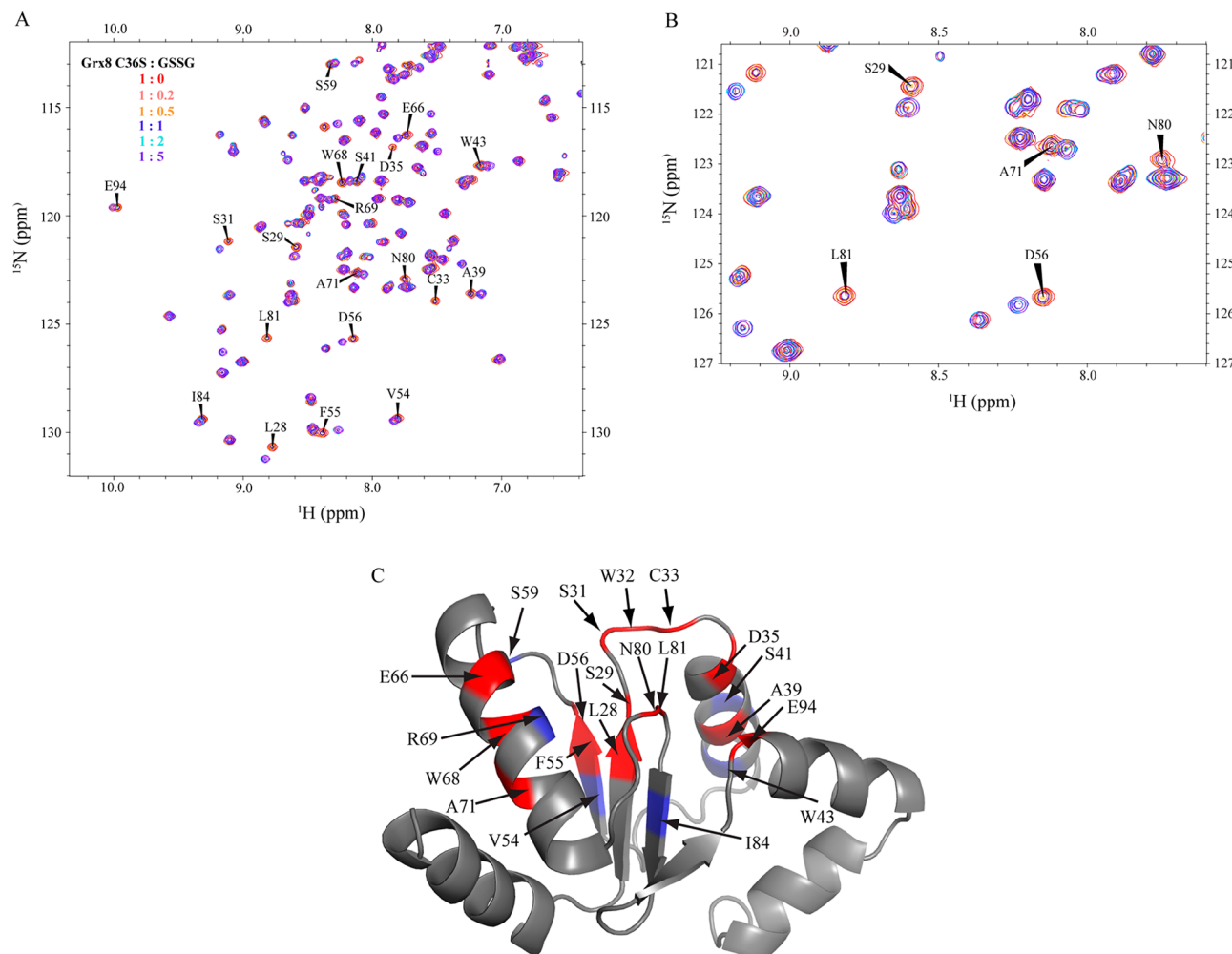


Figure 5. NMR chemical shift perturbation of the C36S mutant by titration of GSSG. (A) Six superimposed ¹⁵N-¹H HSQC spectra of the C36S mutant (0.6 mM) recorded during the titration of GSSG are differently colored. (B) Close-up view of the ¹⁵N-¹H HSQC spectra. (C) Perturbed residues are mapped on the tertiary structure of Grx8. The perturbed residues in slow exchange and those in a stepwise directional manner are red and purple, respectively.

fold. For GSH, both the $k_{\text{cat}}^{\text{app}}$ and $k_{\text{cat}}^{\text{app}}/K_m^{\text{app}}$ values of the D35Y mutant increase by approximately an order of magnitude. The K_m^{app} value of the D35Y mutant for GSH remains similar to wild-type Grx8, whereas the $k_{\text{cat}}^{\text{app}}$ values toward both substrates are increased dramatically.

To study the relationship between the pK_a value and GSH-dependent oxidoreductase activity, we compared the pK_a values of the N-terminal cysteine of Grx8, the D35Y mutant, and Grx1 using a monobromobimane alkylation method (Figure 4).¹⁵ The pK_a value of Cys27 of Grx1 was fitted to 3.9 ± 0.1 , in agreement with a previous report.¹⁵ For Grx8 and the D35Y mutant, the pK_a values of Cys33 were fitted to 7.1 ± 0.1 and 5.7 ± 0.1 , respectively, indicating a 1.4 pH unit decrease of the pK_a value for the D35Y mutant. Thus, the increased activity of the D35Y mutant most likely results from the lowered pK_a value of the N-terminal cysteine in the CPDC motif, which was proposed to enhance the nucleophilicity and leaving group ability of the cysteine thiolate.^{5,6,32}

Mapping the Putative GSH-Recognition Site of Grx8. During the catalytic process, Grx performs a nucleophilic attack at the glutathionylated substrate to form the disulfide bond between Grx and glutathione. To identify the residues that make contact with the glutathione moiety of the glutathionyl-

lated intermediate, glutathione disulfide (GSSG) was titrated to the C36S mutant of Grx8 that was generated to avoid further formation of an intramolecular disulfide bond and release of the glutathione. The glutathionylation of the C36S mutant was previously confirmed by mass spectrometry.²¹ A series of ¹⁵N-¹H HSQC spectra was recorded during the titration (Figure 5A). In total, 15 resonances (Leu28, Ser29, Ser31, Trp32, Cys33, Asp35, Ala39, Phe55, Asp56, Glu66, Trp68, Ala71, Asn80, Leu81, and Glu94) were observed to exhibit slow exchange on the NMR time scale (Figure 5B), whereas six other resonances (Ser41, Trp43, Val54, Ser59, Arg69, and Ile84) shifted in a stepwise directional manner. Mapping the perturbed residues on the tertiary structure of Grx8 showed that they were located at the α_2 , α_3 , β_1 , β_2 , and β_3 strands of Grx8 (Figure 5C). Residues in the CPDC motif and the GSH-recognition site were involved in the perturbation.

Combined with the structural superposition, we mapped the putative GSH-recognition site of Grx8. To check the contribution of these residues to the activity, residues Arg69, Asn80/Leu81, and Glu94/Ser95/Gln96 of Grx8 were mutated to Gln69', Thr80'/Val81', and Asn94'/Asp95'/Asp96' of Grx1, respectively.

Table 3. Kinetic Data of Grx8 and Its Mutants in Two-Substrate Kinetics^a

GSH (mM)	Grx8		Grx8-m3		N80T/L81V		D35Y	
	K_m^{app} (mM)	k_{cat}^{app} ($\times 10^{-3}$ s $^{-1}$)	K_m^{app} (mM)	k_{cat}^{app} ($\times 10^{-3}$ s $^{-1}$)	K_m^{app} (mM)	k_{cat}^{app} ($\times 10^{-3}$ s $^{-1}$)	K_m^{app} (mM)	k_{cat}^{app} ($\times 10^{-3}$ s $^{-1}$)
1.0	0.39 ± 0.033	6.14 ± 0.32	1.90 ± 0.11	435 ± 23.2	2.87 ± 0.65	236 ± 49.5	0.92 ± 0.08	104 ± 7.55
1.5	0.48 ± 0.056	8.88 ± 0.72	2.39 ± 0.15	608 ± 34.3	2.88 ± 0.41	290 ± 37.0	1.24 ± 0.20	152 ± 11.0
2.0	0.62 ± 0.11	11.50 ± 1.42	2.30 ± 0.15	752 ± 44.7	2.89 ± 0.30	333 ± 32.0	1.62 ± 0.33	199 ± 6.3
K_m	13.5 ± 0.89 mM		5.4 ± 0.25 mM		1.4 ± 0.014 mM		18.0 ± 1.0 mM	

^aThe reaction mixture contained 100 mM Tris-HCl (pH 7.5), 0.125 mM NADPH, and 6 µg/mL of GR. The concentration of HEDS was varied from 0.1 to 2.0 mM at a fixed concentration of GSH (1.0, 1.5, or 2.0 mM), and the reactions were started by the addition of Grx8 or the mutants.

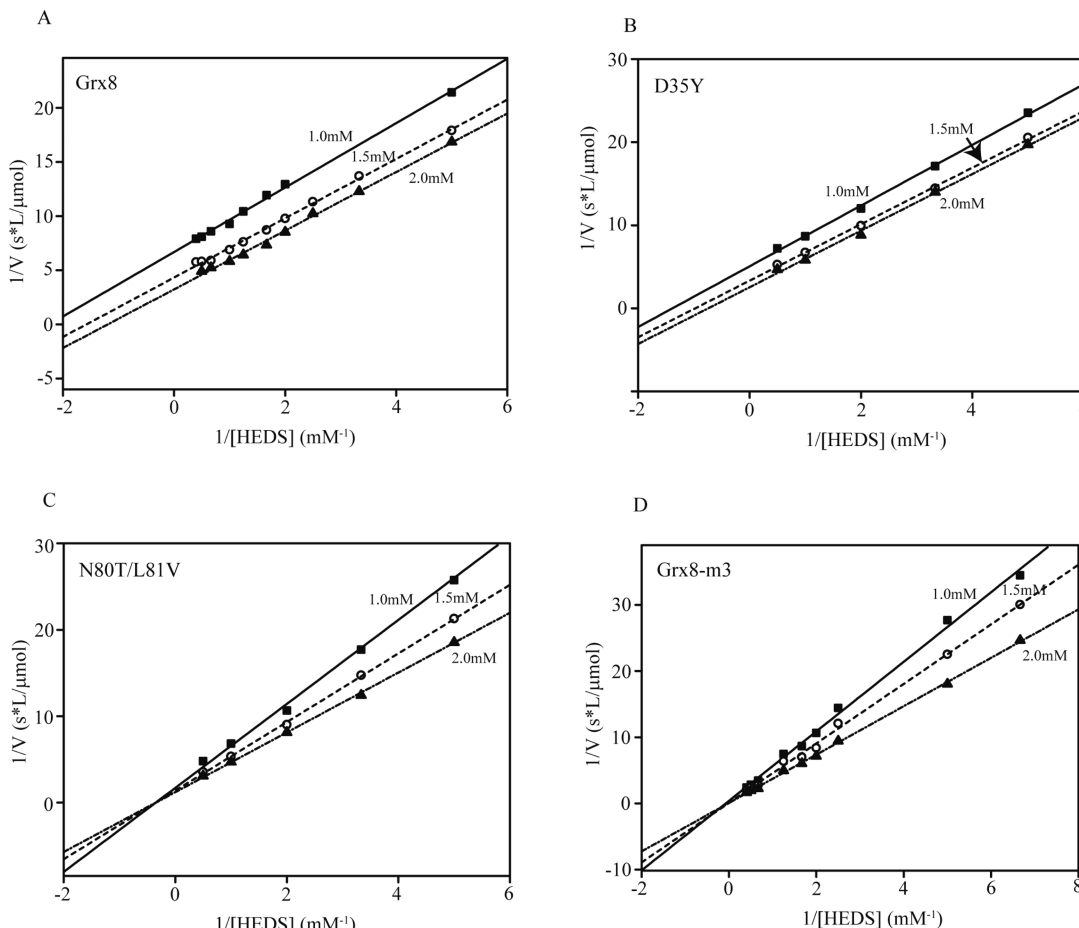


Figure 6. Two-substrate kinetics of Grx8 and its mutants. Representative Lineweaver–Burk plots of (A) Grx8, (B) D35Y mutant, (C) N80T/L81V mutant, and (D) Grx8-m3 are shown. The oxidation of NADPH at 20 °C was recorded spectrophotometrically at 340 nm (for further details, see the Experimental Procedures). The concentration of GSH is labeled in the panels. The apparent steady-state kinetic constants are listed in Table 3.

Elevation of the HEDS Activity of Grx8 Based on Combined Mutations. GSH-dependent oxidoreductase activity of the N80T/L81V and Grx8-m3 (D35Y/N80T/L81V triple mutant) mutants increased remarkably in the HEDS assays (11- and 44-fold, respectively) (Figure 3A), whereas no significant change was detected for the activity of the R69Q single mutant and the E94N/S95D/Q96D triple mutant (data not shown). Furthermore, the apparent kinetic parameters of the N80T/L81V mutant and Grx8-m3 were determined by nonlinear regression of the Michaelis–Menten formula (Table 1).

For HEDS, the K_m^{app} and k_{cat}^{app} values of the N80T/L81V mutant are 4.66- and 28.96-fold higher than that of the wild type, respectively, resulting in an approximately 6-fold higher

catalytic efficiency. Furthermore, Grx8-m3 presents a dramatically increased k_{cat}^{app} value (65.39-fold) and a slightly elevated K_m^{app} value (3.71-fold), resulting in a higher catalytic efficiency (17.63-fold).

For GSH, the K_m^{app} value of the N80T/L81V mutant is half of that of the wild type, whereas the k_{cat}^{app} value is 4.74-fold higher, giving a 10.30-fold higher catalytic efficiency. In contrast, the K_m^{app} value of Grx8-m3 remains almost the same as the wild type, but the k_{cat}^{app} value is increased by 38.60-fold. Consequently, the catalytic efficiency of Grx8-m3 is increased up to 30.22-fold.

Elevated Glutathione S-Transferase Activity of the Grx8 Mutants. Glutathione S-transferases (GSTs) are a class of enzymes that detoxify xenobiotic compounds, leading to

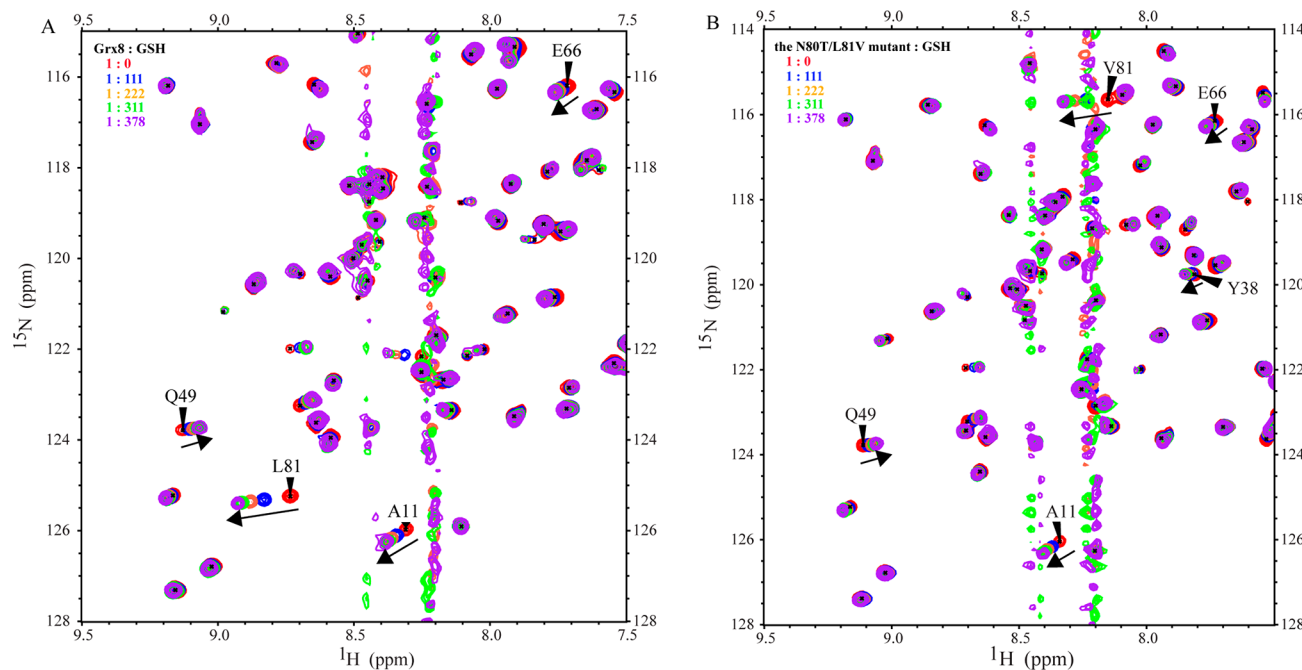


Figure 7. NMR chemical shift perturbation of Grx8 or the N80T/L81V mutant by titration of GSH. (A) Five superimposed ^{15}N - ^1H HSQC spectra of Grx8 (0.45 mM) recorded during the titration of GSH are differently colored. (B) Five superimposed ^{15}N - ^1H HSQC spectra of the N80T/L81V mutant (0.45 mM) recorded during the titration of GSH are differently colored.

formation of glutathionyl adducts of the electrophilic xenobiotics;³³ some Grxs have been reported to display GST activity.³⁴ Using Grx1 as a control, we detected the GST activities of the wild-type Grx8 and its mutants for the conversion of 4-chloro-7-nitro-2,1,3-benzoxadiazole (NBD-Cl) to glutathionylated NBD. As shown in Figure 3B, the N80T/L81V mutant possesses GST activity that is 5.2-fold of that of the wild type or 64% of that of Grx1. In addition, the activity of the D35Y mutant is about 2-fold of that of the wild type, whereas Grx8-m3 has a GST activity comparable to that of Grx1.

Two-Substrate Kinetics of Grx8 and Its Mutants. To characterize the kinetic features of GSH-dependent oxidoreduction further, we studied the two-substrate kinetics of Grx8 and its mutants. The concentrations of HEDS were varied from 0.1 to 2.0 mM at fixed concentrations of GSH (1.0, 1.5, and 2.0 mM). A series of apparent kinetic data of Grx8 and its mutants for HEDS was determined (Table 3).

When the kinetic data of wild-type Grx8 were linearized by the Lineweaver–Burk equation, a series of parallel lines was observed in the double-reciprocal plots of the initial reaction velocities and HEDS concentrations (Figure 6A), indicating a ping-pong mechanism for Grx8. Similarly, the lines are also parallel for the D35Y mutant (Figure 6B). We then built the secondary plots with the intercept values of the first plot ($K_m^B/V_m \times 1/[GSH] + 1/V_m$) versus the reciprocal of the GSH concentration to obtain the true K_m value. The K_m values of Grx8 and the D35Y mutant toward GSH were fitted to 13.5 ± 0.89 and 18.0 ± 1.0 mM, respectively (Table 3). However, the double-reciprocal plots of the N80T/L81V and Grx8-m3 mutants exhibited the intersecting lines, consistent with a sequential mechanism (Figure 6C,D). Similarly, the secondary plots were built with the intercept values of the first plot ($K_m^B/V_m \times 1/[GSH] + 1/V_m$) versus the reciprocal of the GSH concentration and gave K_m values of 1.4 ± 0.014 and 5.4 ± 0.25 mM for the N80T/L81V and Grx8-m3 mutants, respectively.

DISCUSSION

Residues Asp35, Asn80, and Leu81 Are Responsible for the Low Activity of Grx8. It has long been known that many oxidoreductases with a CXXC motif have a pK_a value of the catalytic cysteine that is lower than that of free cysteine ($pK_a \sim 9$).^{35,36} For the previously reported Grxs, the pK_a values of the catalytic cysteine are less than 6.^{13,31,36,37} When the reactions take place at physiological pH, the lowering of the pK_a value of the catalytic cysteine elevates the reaction rate by increasing the concentration of thiolate anion. It has also been demonstrated that the intervening residues in the CXXC motif influence the pK_a value of the catalytic cysteine.³⁸ In our study, the pK_a value of the catalytic cysteine of the D35Y mutant was found to decrease by 1.4 pH units. However, the catalytic activity of the D35Y mutant is 10-fold of that of the wild-type Grx8 (Figure 3A). For thiol–disulfide exchange reactions, when the pK_a value is lowered by one pH unit, the second-order rate constant increases by a factor of 4.^{5,6,32} Thus, the pK_a value shift predicts a 7-fold rate enhancement in specific activity ($4\Delta pK_a = 4^{1.4} = 7.0$ -fold), accounting for the majority of the distinction in the catalytic efficiency between the D35Y mutant and Grx8.

Because of the effects on the nucleophilicity and leaving group ability of the thiolate, a low pK_a value of the N-terminal cysteine thiolate anion of Grxs could accelerate the reaction.^{4–7} Tyr in the CPYC motif of Grx1 and Grx2 scarcely influences the electrostatic charge circumstance of the N-terminal cysteine. The high pK_a value of the catalytic cysteine of Grx8 might be due to Asp35 in the CPDC motif, which affects the catalytic cysteine thiolate stability via electrostatic repulsion between the negatively charged Asp35 and Cys33 thiolate. Thus, compared with Grx1 and Grx2, Grx8 possesses a dramatically decreased GSH-dependent oxidoreductase activity. Moreover, substitution of D35Y would increase the stability of catalytic cysteine thiolate and significantly elevate the catalytic efficiency.

GSH-dependent oxidoreductase activity of the N80T/L81V mutant is elevated 11-fold compared to that of wild-type Grx8. This could be attributed to the accelerated formation of the glutathionylated intermediate of the N80T/L81V mutant. As shown in Figure 1B,C, residues at the GSH-recognition site of glutathionylated Grx1 or Grx2 accommodate the GSH molecule well. The side chains of Asn80 and Leu81 of Grx8 are slightly larger than those of the corresponding Thr and Val residues of Grx1 and Grx2 (Figure 1B,C). Thus, in glutathionylated Grx8, the steric hindrance caused by the side chains would keep the main chains of Asn80 and Leu81 away from that of GSH. Mutations of N80T/L81V could facilitate the formation of hydrogen bonds and the glutathionylated intermediate and consequently increase the catalytic efficiency. Thus, it is not surprising that the catalytic activity of the D35Y/N80T/L81V mutant is increased 44-fold (Figure 3A). Besides, the GST activity of the N80T/L81V mutant was dramatically elevated as well (Figure 3B), indicating that residues for GSH recognition also play an important role in the GST activity. We hypothesized that the Thr and Val residues at the GSH-recognition site would be critical for the activation of the thiol group of reduced glutathione.

Catalytic Mechanisms of Grx8 and Its Mutants. It seems that upon the mutation of two key residues, Asn80 and Leu81 at the GSH-recognition site, the ping–pong mechanism of Grxs was switched to a sequential one. The catalytic reaction of Grxs has been described as a ping–pong mechanism for years,¹² whereas the sequential mechanism was proposed for several Grxs toward HEDS and GSH.^{13–15} In the HEDS assay, HEDS and GSH were preincubated to form the real substrate, glutathionylated β -mercaptoethanol (β -ME-SSG). Human Grx and yeast Grx7 displayed a sequential mechanism toward HEDS and GSH, and this was attributed to the rate-limiting formation of β -ME-SSG.¹² As we know, the key point to distinguish the sequential mechanism from the ping–pong one is whether the ternary complex forms during the reaction process. The sequential mechanism proposed that the two substrates bind to the enzyme simultaneously or successively without release of the product. Therefore, we studied the interaction between Grx8 or the N80T/L81V mutant and reduced glutathione by performing NMR chemical shift perturbation and GSH analogue inhibition assays.

The reduced glutathione was titrated to Grx8 or the N80T/L81V mutant up to 378-fold, and five ^{15}N – ^1H HSQC spectra were recorded during the titration (Figure 7). There were four resonances shifted for Grx8 (A11, Q49, E66, and L81), and five resonances shifted for the N80T/L81V mutant (A11, Y38, Q49, E66, and V81). The K_d values were fitted to be 126.4 ± 7.9 and 143.6 ± 13.5 mM for Grx8 and the N80T/L81V mutant, respectively, suggesting a nonspecific interaction between reduced glutathione and the wild-type Grx8 or even the N80T/L81V mutant.

Furthermore, we used S-methyl glutathione, an analogue of reduced glutathione, to determine if it could inhibit the GST activity of Grx8 or the N80T/L81V mutant. Yeast Grx1 and Grx2 have been reported to display GST activity.³⁴ The N80T/L81V mutant displayed GST activity comparable to that of Grx1 (Figure 3B). Upon the addition of S-methyl glutathione, the GST activity of Grx1 was decreased by half, whereas the activities of Grx8 and the N80T/L81V mutant were not affected even at a millimolar concentration of the analogue (Figure 8). In fact, previous reports indicated that S-methyl glutathione did not inhibit the enzymatic reaction of human

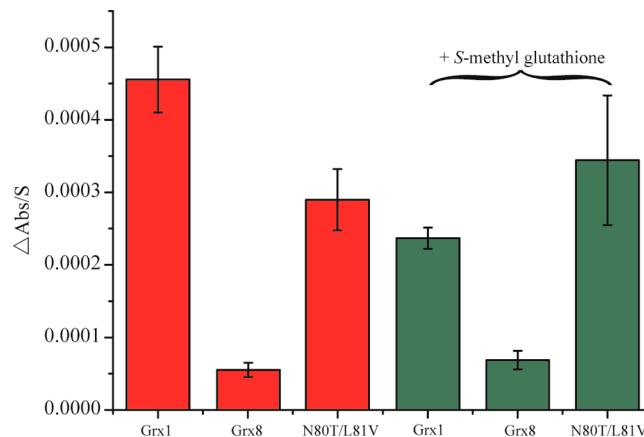


Figure 8. S-Methyl glutathione inhibition assays of Grx8 and the N80T/L81V mutant. GST activities are displayed in green and red histograms for the assays with and without S-methyl glutathione, respectively.

Grx1 and Grx2.^{6,32} These findings are in agreement with the demonstration that enzyme–substrate complexes did not form during the reaction.⁷

As shown by Figure 1B,C, the side chains of Asn80 and Leu81 of Grx8 are larger than those of Thr74 and Val75 in Grx1 and Grx2; thus, steric hindrance may influence the formation of hydrogen bonds between the main chains of Grx8 and the glutathione moiety in the glutathionylated intermediate. After mutations, the steric hindrance would be eliminated, and the glutathionylated form of the N80T/L81V mutant could be produced more efficiently. Consequently, the mutations would lower the concentration dependency of the second step, reduction of the glutathionylated intermediate by GSH, in accordance with the lower K_m value of the N80T/L81V mutant toward GSH (Tables 1 and 3). Moreover, before Grxs was added to the reaction mixture, HEDS and GSH were preincubated to form the real substrate, β -ME-SSG. The nonenzymatic reaction rate for HEDS and GSH is very low. If the N80T/L81V mutant in the glutathionylated form is produced more rapidly because of the elimination of steric hindrance, then the supply of β -ME-SSG would be insufficient and the formation of β -ME-SSG would be the rate-limiting step. Because the concentration of β -ME-SSG was proportional to that of HEDS, the insufficiency would be more obvious when the initial concentration of HEDS is low. This would affect the slope of the lines in the double-reciprocal plots of the initial reaction velocities and HEDS concentrations in two-substrate kinetics. Thus, the sequential mechanism of the N80T/L81V mutant deduced from two-substrate kinetics is not convincing. The sequential mechanism employed by human Grx has been proposed to result from the rate-limiting formation of β -ME-SSG;¹² however, alternative interpretations have been proposed.³⁹ Nevertheless, the catalytic mechanism of the Grxs has never been explained by reversible binding of reduced glutathione.

In summary, we have reported the solution structure of yeast Grx8, which is one of the few dithiol Grxs with a low HEDS activity. Structural comparison of Grx8 and the other two yeast dithiol Grxs indicated variations in the CXXC motif and GSH-recognition site. The Asp35, Asn80, and Leu81 residues are responsible for the low activity of Grx8, and the mutations of these residues consequently increase the HEDS and GST activities. In addition, we demonstrated that the wild-type Grx8

and its mutants adopt a ping–pong mechanism of catalysis. All together, these findings provide insights into the structure and catalytic mechanism of Grxs.

■ ASSOCIATED CONTENT

Accession Codes

Structural coordinates of yeast Grx8 have been deposited in the Protein Data Bank (accession code 2M80).

■ AUTHOR INFORMATION

Corresponding Authors

*(C.Z.Z.) Tel: 86-551-63600406; Fax: 86-551-63600406; E-mail: zcz@ustc.edu.cn.

*(Y.S.) Tel: 86-551-63607464; Fax: 86-551-63600441; E-mail: yyshi@ustc.edu.cn.

Funding

This work was financially supported by the National Basic Research Program of China (973 Program, grant nos. 2011CB966302, 2012CB911000, and 2011CB911104) and the Chinese National Natural Science Foundation (grant no. 31330018).

Notes

The authors declare no competing financial interest.

■ ACKNOWLEDGMENTS

We thank Prof. Qingguo Gong, Prof. Ke Ruan, Dr. Zhenwei Song, Dr. Ming Luo, and Dr. Su Qin for helpful advice and discussions. We thank Dr. F. Delaglio and Prof. A. Bax for providing the software NMRPipe, Prof. T. D. Goddard and Prof. D. G. Kneller for providing Sparky, Prof. A. T. Brünger for providing the program CNS, Dr. R. Koradi and Prof. K. Wüthrich for providing MOLMOL, and Warren L. DeLano for providing PyMOL.

■ ABBREVIATIONS USED

Grx, glutaredoxin; GR, glutathione reductase; GSH, reduced glutathione; GSSG, oxidized glutathione, glutathione disulfide; HEDS, β -hydroxyethyl disulfide; GS-SCys, L-cysteine-glutathione disulfide; β -ME-SSG, glutathionylated β -mercaptoethanol; MES, 2-(N-morpholino)ethanesulfonic acid hydrate; Grx_{re}, reduced glutaredoxin; Grx_{GS}, glutathionylated glutaredoxin; Grx_{ox}, oxidized glutaredoxin; rmsd, root-mean-square deviation; PDB, Protein Data Bank; NMR, nuclear magnetic resonance; HSQC, heteronuclear single quantum correlation; TOCSY, total correlation spectroscopy; NOE, nuclear Overhauser effect; NOESY, NOE spectroscopy

■ REFERENCES

- (1) Luikenhuis, S., Perrone, G., Dawes, I. W., and Grant, C. M. (1998) The yeast *Saccharomyces cerevisiae* contains two glutaredoxin genes that are required for protection against reactive oxygen species. *Mol. Biol. Cell* 9, 1081–1091.
- (2) Li, H., Mapolelo, D. T., Dingra, N. N., Naik, S. G., Lees, N. S., Hoffman, B. M., Riggs-Gelasco, P. J., Huynh, B. H., Johnson, M. K., and Outten, C. E. (2009) The yeast iron regulatory proteins Grx3/4 and Fra2 form heterodimeric complexes containing a [2Fe–2S] cluster with cysteinyl and histidyl ligation. *Biochemistry* 48, 9569–9581.
- (3) Holmgren, A., and Aslund, F. (1995) Glutaredoxin. *Methods Enzymol.* 252, 283–292.
- (4) Gilbert, H. F. (1990) Molecular and cellular aspects of thiol-disulfide exchange. *Adv. Enzymol. Relat. Areas Mol. Biol.* 63, 69–172.
- (5) Szajewski, R. P., and Whitesides, G. M. (1980) Rate constants and equilibrium-constants for thiol-disulfide interchange reactions involving oxidized glutathione. *J. Am. Chem. Soc.* 102, 2011–2026.
- (6) Gallogly, M. M., Starke, D. W., Leonberg, A. K., Ospina, S. M., and Mieyal, J. J. (2008) Kinetic and mechanistic characterization and versatile catalytic properties of mammalian glutaredoxin 2: Implications for intracellular roles. *Biochemistry* 47, 11144–11157.
- (7) Gallogly, M. M., Starke, D. W., and Mieyal, J. J. (2009) Mechanistic and kinetic details of catalysis of thiol-disulfide exchange by glutaredoxins and potential mechanisms of regulation. *Antioxid. Redox Signaling* 11, 1059–1081.
- (8) Nordstrand, K., Åslund, F., Holmgren, A., Otting, G., and Berndt, K. D. (1999) NMR structure of *Escherichia coli* glutaredoxin 3-glutathione mixed disulfide complex: implications for the enzymatic mechanism. *J. Mol. Biol.* 286, 541–552.
- (9) Yu, J., Zhang, N. N., Yin, P. D., Cui, P. X., and Zhou, C. Z. (2008) Glutathionylation-triggered conformational changes of glutaredoxin Grx1 from the yeast *Saccharomyces cerevisiae*. *Proteins* 72, 1077–1083.
- (10) Yang, Y., Jao, S., Nanduri, S., Starke, D. W., Mieyal, J. J., and Qin, J. (1998) Reactivity of the human thioltransferase (glutaredoxin) C7S, C25S, C78S, C82S mutant and NMR solution structure of its glutathionyl mixed disulfide intermediate reflect catalytic specificity. *Biochemistry* 37, 17145–17156.
- (11) Zaffagnini, M., Bedhomme, M., Marchand, C. H., Couturier, J. R., Gao, X. H., Rouhier, N., Trost, P., and Lemaire, S. P. (2012) Glutaredoxin s12: Unique properties for redox signaling. *Antioxid. Redox Signaling* 16, 17–32.
- (12) Gravina, S. A., and Mieyal, J. J. (1993) Thioltransferase is a specific glutathionyl mixed disulfide oxidoreductase. *Biochemistry* 32, 3368–3376.
- (13) Mieyal, J. J., Starke, D. W., Gravina, S. A., and Hocevar, B. A. (1991) Thioltransferase in human red blood cells: Kinetics and equilibrium. *Biochemistry* 30, 8883–8891.
- (14) Mesecke, N., Mittler, S., Eckers, E., Herrmann, J. M., and Deponte, M. (2008) Two novel monothiol glutaredoxins from *Saccharomyces cerevisiae* provide further insight into iron-sulfur cluster binding, oligomerization, and enzymatic activity of glutaredoxins. *Biochemistry* 47, 1452–1463.
- (15) Discola, K. F., de Oliveira, M. A., Rosa Cussiol, J. R., Monteiro, G., Barcena, J. A., Porras, P., Padilla, C. A., Guimaraes, B. G., and Netto, L. E. (2009) Structural aspects of the distinct biochemical properties of glutaredoxin 1 and glutaredoxin 2 from *Saccharomyces cerevisiae*. *J. Mol. Biol.* 385, 889–901.
- (16) Li, W. F., Yu, J., Ma, X. X., Teng, Y. B., Luo, M., Tang, Y. J., and Zhou, C. Z. (2010) Structural basis for the different activities of yeast Grx1 and Grx2. *Biochim. Biophys. Acta* 1804, 1542–1547.
- (17) Rodriguez-Manzaneque, M. T., Ros, J., Cabisco, E., Sorribas, A., and Herrero, E. (1999) Grx5 glutaredoxin plays a central role in protection against protein oxidative damage in *Saccharomyces cerevisiae*. *Mol. Cell. Biol.* 19, 8180–8190.
- (18) Mesecke, N., Spang, A., Deponte, M., and Herrmann, J. M. (2008) A novel group of glutaredoxins in the cis-Golgi critical for oxidative stress resistance. *Mol. Biol. Cell* 19, 2673–2680.
- (19) Ojeda, L., Keller, G., Muhlenhoff, U., Rutherford, J. C., Lill, R., and Winge, D. R. (2006) Role of glutaredoxin-3 and glutaredoxin-4 in the iron regulation of the Aft1 transcriptional activator in *Saccharomyces cerevisiae*. *J. Biol. Chem.* 281, 17661–17669.
- (20) Luo, M., Jiang, Y. L., Ma, X. X., Tang, Y. J., He, Y. X., Yu, J., Zhang, R. G., Chen, Y., and Zhou, C. Z. (2010) Structural and biochemical characterization of yeast monothiol glutaredoxin Grx6. *J. Mol. Biol.* 398, 614–622.
- (21) Eckers, E., Bien, M., Stroobant, V., Herrmann, J. M., and Deponte, M. (2009) Biochemical characterization of dithiol glutaredoxin 8 from *Saccharomyces cerevisiae*: The catalytic redox mechanism redux. *Biochemistry* 48, 1410–1423.
- (22) Delaglio, F., Grzesiek, S., Vuister, G. W., Zhu, G., Pfeifer, J., and Bax, A. (1995) NMRPipe: A multidimensional spectral processing system based on UNIX pipes. *J. Biomol. NMR* 6, 277–293.

- (23) Goddard, T. D., and Kneller, D. G. (2006) *Sparky 3*, University of California, San Francisco, CA.
- (24) Shen, Y., Delaglio, F., Cornilescu, G., and Bax, A. (2009) TALOS+: A hybrid method for predicting protein backbone torsion angles from NMR chemical shifts. *J. Biomol. NMR* 44, 213–223.
- (25) Brunger, A. T., Adams, P. D., Clore, G. M., DeLano, W. L., Gros, P., Grosse-Kunstleve, R. W., Jiang, J. S., Kuszewski, J., Nilges, M., Pannu, N. S., Read, R. J., Rice, L. M., Simonson, T., and Warren, G. L. (1998) Crystallography & NMR system: A new software suite for macromolecular structure determination. *Acta Crystallogr., Sect. D: Biol. Crystallogr.* 54, 905–921.
- (26) Laskowski, R. A., Rullmann, J. A., MacArthur, M. W., Kaptein, R., and Thornton, J. M. (1996) AQUA and PROCHECK-NMR: Programs for checking the quality of protein structures solved by NMR. *J. Biomol. NMR* 8, 477–486.
- (27) Koradi, R., Billeter, M., and Wuthrich, K. (1996) MOLMOL: A program for display and analysis of macromolecular structures. *J. Mol. Graphics* 14, 29–32.
- (28) Ricci, G., Caccuri, A. M., Lo Bello, M., Pastore, A., Piemonte, F., and Federici, G. (1994) Colorimetric and fluorometric assays of glutathione transferase based on 7-chloro-4-nitrobenzo-2-oxa-1,3-diazole. *Anal. Biochem.* 218, 463–465.
- (29) Hakansson, K. O., and Winther, J. R. (2007) Structure of glutaredoxin Grx1p C30S mutant from yeast. *Acta Crystallogr., Sect. D: Biol. Crystallogr.* 63, 288–294.
- (30) Sun, C., Berardi, M. J., and Bushweller, J. H. (1998) The NMR solution structure of human glutaredoxin in the fully reduced form. *J. Mol. Biol.* 280, 687–701.
- (31) Foloppe, N., Sagemark, J., Nordstrand, K., Berndt, K. D., and Nilsson, L. (2001) Structure, dynamics and electrostatics of the active site of glutaredoxin 3 from *Escherichia coli*: Comparison with functionally related proteins. *J. Mol. Biol.* 310, 449–470.
- (32) Srinivasan, U., Mieyal, P. A., and Mieyal, J. J. (1997) pH profiles indicative of rate-limiting nucleophilic displacement in thioltransferase catalysis. *Biochemistry* 36, 3199–3206.
- (33) Sheehan, D., Meade, G., Foley, V. M., and Dowd, C. A. (2001) Structure, function and evolution of glutathione transferases: Implications for classification of non-mammalian members of an ancient enzyme superfamily. *Biochem. J.* 360, 1–16.
- (34) Collinson, E. J., and Grant, C. M. (2003) Role of yeast glutaredoxins as glutathione S-transferases. *J. Biol. Chem.* 278, 22492–22497.
- (35) Mossner, E., Huber-Wunderlich, M., and Glockshuber, R. (1998) Characterization of *Escherichia coli* thioredoxin variants mimicking the active-sites of other thiol/disulfide oxidoreductases. *Protein Sci.* 7, 1233–1244.
- (36) Foloppe, N., and Nilsson, L. (2007) Stabilization of the catalytic thiolate in a mammalian glutaredoxin: Structure, dynamics and electrostatics of reduced pig glutaredoxin and its mutants. *J. Mol. Biol.* 372, 798–816.
- (37) Nordstrand, K., Aslund, F., Meunier, S., Holmgren, A., Otting, G., and Berndt, K. D. (1999) Direct NMR observation of the Cys-14 thiol proton of reduced *Escherichia coli* glutaredoxin-3 supports the presence of an active site thiol-thiolate hydrogen bond. *FEBS Lett.* 449, 196–200.
- (38) Chivers, P. T., Prehoda, K. E., and Raines, R. T. (1997) The CXXC motif: A rheostat in the active site. *Biochemistry* 36, 4061–4066.
- (39) Deponte, M. (2013) Glutathione catalysis and the reaction mechanisms of glutathione-dependent enzymes. *Biochim. Biophys. Acta* 1830, 3217–3266.